Electrochemical Impedance Spectroscopic Study of the Electronic and Ionic Transport Properties of NiF$_2$/C Composites

Yue-Li Shi[1], Ming-Fang Shen[1], Shou-Dong Xu[1], Xiang-Yun Qiu[1], Li Jiang[1], Ying-Huai Qiang[1], Quan-Chao Zhuang[1,], Shi-Gang Sun[2]*

[1] Li-ion Batteries Lab, School of Materials Science and Engineering, China University of Mining and technology, Xuzhou 221116, China
[2] State Key Lab of Physical Chemistry of Solid Surfaces, Department of Chemistry, College of Chemistry and Chemical Engineering, Xiamen University, Xiamen 361005, China
[*]E-mail: zhuangquanchao@126.com

NiF$_2$/C composites were prepared through high energy mechanical milling, and the cyclic performance was characterized by discharge-charge measurements. Electrochemical impedance spectra (EIS) for NiF$_2$/C electrode were obtained at different potentials during initial discharge-charge cycle. The results revealed the typical EIS characteristics appeared with three semicircles in the Nyquist diagram at 1.6 V. An equivalent circuit was proposed to simulate the experimental EIS data, and it was found that the high frequency semicircle (HFS) is mainly caused by lithium-ion through the SEI film on the electrode surface, the middle frequency semicircle (MFS) should be related to the Schottky contact between NiF$_2$ and conductive agents, which may be the important feature of such composites materials with big band gap, Besides the low frequency arc (LFA) was observed as the charge transfer step. Consequently a modified model was proposed to explain the impedance response of NiF$_2$/C electrode for lithium ion batteries.

1. INTRODUCTION

Rechargeable lithium ion batteries (LIBs) are currently the preferred energy storage devices in many portable electronic devices such as cell phones, digital cameras/videos, and laptop computers due to their longer cycling life and higher energy density than other rechargeable batteries [1]. Moreover, it has been extensively studied for use in new applications such as electric vehicles (EVs), hybrid electric vehicles (HEVs), and power backups. However, both existing and new emerging applications demand even better performance in terms of energy density, power, safety, price and

environmental impact. At the present time, the layered intercalation compound $LiCoO_2$ [2] is utilized as a cathode in most commercial lithium ion batteries. Recently, more developments are based on cathodic insertion materials, such as $LiMn_2O_4$ [3, 4] and $LiFePO_4$ [5]. The reversible homogeneous intercalation and deintercalation reaction of these insertion materials gives excellent cycling performance but involves at most a single electron transfer per formula unit, corresponding to a limited capacity [6]. How to increase the specific energy density of LIBs has recently become one of the most attractive topics of both scientific and industrial interests.

In 2000, Poizot et al. [7] reported that lithium can be stored reversibly in transition metal oxides through the heterogeneous conversion reaction:

$$Li+TMO \rightarrow Li_2O+TM \tag{1}$$

Where TM=Co, Fe, Ni, Cu, and so on. In contrast to the stable framework of the intercalation materials during cycling, the transition metal oxides are reduced in a conversion reaction to small metal clusters with the oxygen reacting with Li to form Li_2O. Later, reversible lithium storage was also observed in transition metal fluorides as well as sulfides, nitrides, selenides and phosphides [8-16]. As opposed to intercalation reactions, the reversible conversion process enables the full redox utilization of the transition metal and has 2-4 times the specific capacity of intercalation compounds as high as 600-1000 mAh/g [17]. Because the potential of conversion reaction is directly proportional to the strength of the ionic bond, only metal fluorides have a high enough potential to be used as lithium-ion cathodes. Unfortunately, there are two main barriers which have inhibited the use of metal fluoride electrodes as follows: (1) the ionic nature of the metal-fluorine bond corresponding wide band gap results in electronically insulating behavior such as potential delay and poor energy efficiency. (2) The variation of volume upon cycling possibly induces the loss of electrical contact of the electrode material with the current collector, and the decomposition of SEI film leading to poor capacity retention [18-20].

To overcome these problems, the knowledge of electronic and ionic transports as well as the charge transfer reaction at the electrode/electrolyte interface is required to better understand electrochemical behaviors since they govern the charge capacity and rate capability, and would undoubtedly facilitate further electrode optimization. However, during the past years the main focus has been on understanding the properties of bulk active material, such as the atomic and electronic structure of the active material and their eventual changes during the charge-discharge process [18, 21, 22], and the scientific literature is rather scarce on the study of electronic and ionic transport properties of the electrode materials versus their electrochemical behavior.

Electrochemical impedance spectroscopy (EIS) is one of the most important, highly resolved electroanalytical techniques which may provide a unique information about the nature of electrode processes related to a wide range of time constants (demonstrated in terms of frequencies in EIS). In the past decades, EIS has been widely applied to the analysis of the electrochemical lithium intercalation into the carbonaceous materials and transition metal oxides [23-41]. It should also be applied to the analysis of the lithiation and delithiation conversion mechanisms of transition metal compounds, however that is rarely reported. In this study, NiF_2/C composites were prepared through

high energy mechanical milling, the charge-discharge cycling performance of the material was characterized, and its kinetic properties were studied by EIS. Special emphasis is placed on the ionic and electronic transport properties of the NiF_2/C composites electrode in the first lithiation-delithiation process.

2. EXPERIMENTAL METHODS

2.1. Materials Preparation

NiF_2/C composites were prepared by high-energy milling of NiF_2 (Aladdin Co. Shanghai, China) with carbon black and graphite (Shanshan Co. Shanghai, China). Stoichiometric mixtures [NiF_2/carbon black/graphite = 5:2:1 (w/w)] were placed inside a steel milling cell with steel balls. Milling was performed for 3 h in a high-energy milling machine (QM-3SP2, Nanjing NanDa Instrument Plant, Nanjing, China) at 450 rpm.

2.2. Electrochemical Characterization

The positive electrode composition was 90 wt% NiF_2/C composites powder, 10 wt% ployvinylidene fluoride binder (Kynar FLEX 2801, Elf-atochem, USA), and an aluminum foil was used as current collector. The electrolyte was 1 $mol \cdot L^{-1}$ $LiPF_6$-EC:DEC:DMC (volume ratio 1:1:1, Guotaihuarong Co., Zhangjiagang, China).

All electrochemical impedance experiments were conducted in a three-electrode glass cell with Li foils as both auxiliary and reference electrodes using an electrochemical work station (CHI660D, Chenhua Ltd Co., Shanghai, China). The amplitude of ac perturbation signal was 5 mV and the frequency range was from 10^5 to 10^{-2} Hz. The electrode was equilibrated for 1 h before EIS measurements. The impedance data were analyzed using Zview software. Charge-discharge cycles were carried out at 0.1 C in a 2025 coin cell using lithium metal as the second electrode, over a potential range between 0.5 and 4.0 V.

2.3. X-ray Diffraction

The phase identification was carried out by powder XRD using Cu Kα radiation on a Rigaku D/Max-3B diffractometer. Diffraction data were collected by step scanning over an angular range of 10–60° with a step width of 0.01° (35 KV, 30 mA).

3. RESULTS AND DISCUSSION

The joint committee for powder diffraction studies (JCPDS) of NiF_2 (PDF: 25-0579) and XRD patterns of NiF_2 and NiF_2/C composites are shown in Figure 1. All patterns are in good agreement with

the PDF standard, and all the diffraction peaks could be indexed based on the orthorhombic structure, and graphite phase (marked by asterisk in Fig. 1a) exists in the composites, indicating that no significant structural changes and impurity phases were introduced during the milling process. However, a noticeable broadening of the Bragg peaks is observed, suggesting that the particle size decreased considerably on high-energy milling.
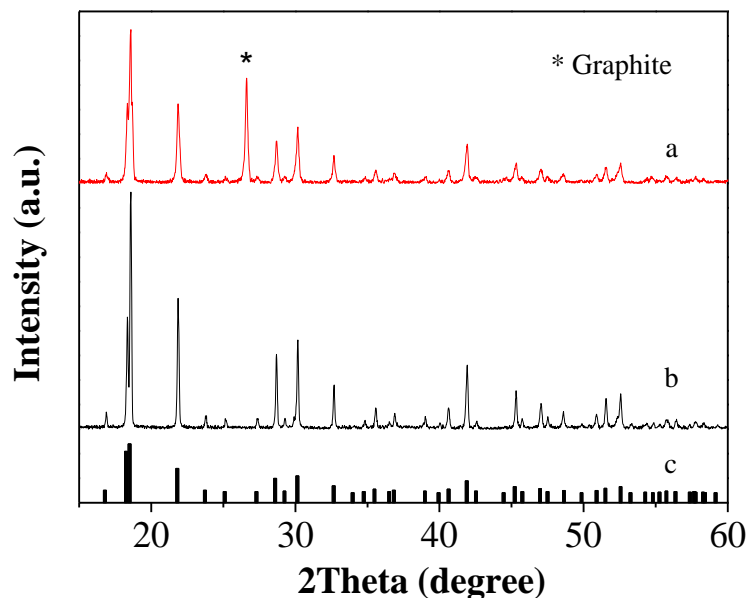
Figure 1. XRD patterns of (a) NiF_2/C composite; (b) commercial NiF_2; (c) standard NiF_2 (PDF: 25-0579).

Figure 2 illustrates the 1st, 2nd and 10th charge-discharge curves of Li/(NiF_2/C composites) cells (Fig. 2a) and the differential capacity curves of Li/(NiF_2/C composites) cells upon the first two cycles (Fig. 2b). The voltage profile exhibits its electrochemical activity.
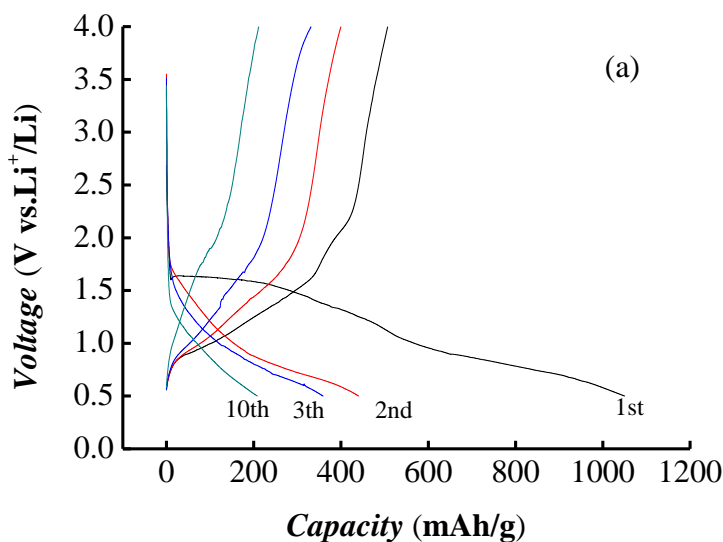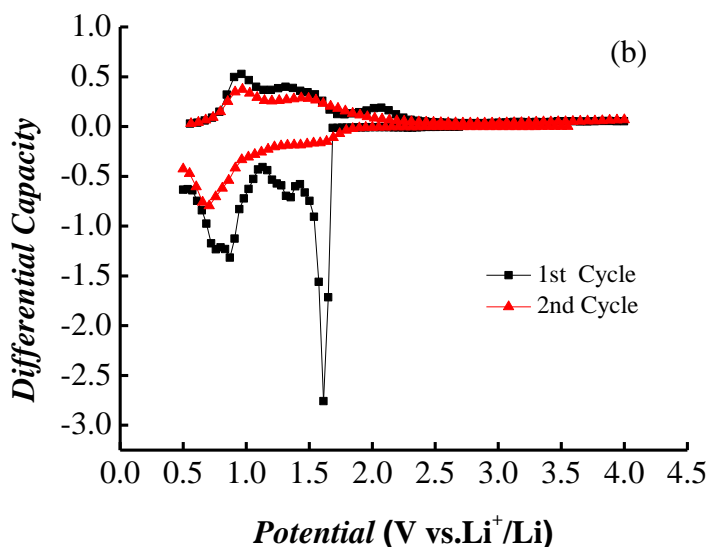
Figure 2. (a) Discharge/charge profiles of Li/(NiF$_2$/C composites) cell (1th, 2nd, 3th, and 10th cycle); (b) Differential capacity curves of Li/(NiF$_2$/C composites) cell. The range of voltage: 4.0 - 0.5 V, the current density: 5.5 mAh/g.

A long plateau at 1.6 V is observed, which is far below the theoretical operating potential (2.96 V) [42]. After which, the voltage decreases gradually to ~1.0 V, and a slope region is then observed. The first discharge capacity amounts to ~1100 mAh/g, but the capacity fades fast in the subsequent charge-discharge process, the capacity of second cycle is only half the capacity of the former's, eventually it drops to 200 mAh/g at the tenth cycle, indicating the poor capacity retention of NiF$_2$/C electrode. This behavior is similar to that found by Li et al. [43]. The initial discharge capacity of 1100 mAh/g is quite higher than the theoretical value (554 mAh/g). Similar phenomena were also observed in some other transition metal fluorides and could be explained by an interfacial interaction of lithium within the M/LiX matrix, possibly leading to a distinct local charging, as proposed by Maier' group [44], in addition to the formation of a solid electrolyte interphase (SEI) film on electrode surface [45]. The differential capacity curves in Fig. 2b appeared two peaks at 1.6 V and 0.8 V in the first discharge process, corresponding to the plateau and slope respectively. The plateau in the voltage profile is an indication of a phase transformation reaction, and its capacity (~500 mAh/g) was close to the theoretical value. Therefore, the plateau at the first discharge cycle should be attributed to the reaction [46]:

$$2Li+NiF_2 \rightarrow 2LiF+Ni \qquad\qquad\qquad\qquad\qquad\qquad\qquad\qquad (2)$$

In addition, the reduction peak (1.6 V) shows severe irreversibility during the second cycle, which maybe associated with the formation of SEI film in the previous cycle. The sloped region below 1V denoted an extra reversible capacity, probably due to Li storage in the newly formed LiF/Ni boundaries, or "interfacial interaction of lithium" mentioned above [44]. During the first charge process, it appears three peaks at the potential of 1.0 V, 1.5 V and 2.0 V (Fig. 2b), which is slightly different from the previous study with only one oxidation peak near 2.2 V [46], the two oxidation

peaks (1.0V & 1.5V) are probably related to the converse of the interfacial interaction of lithium and decomposition process of SEI film [47, 48].
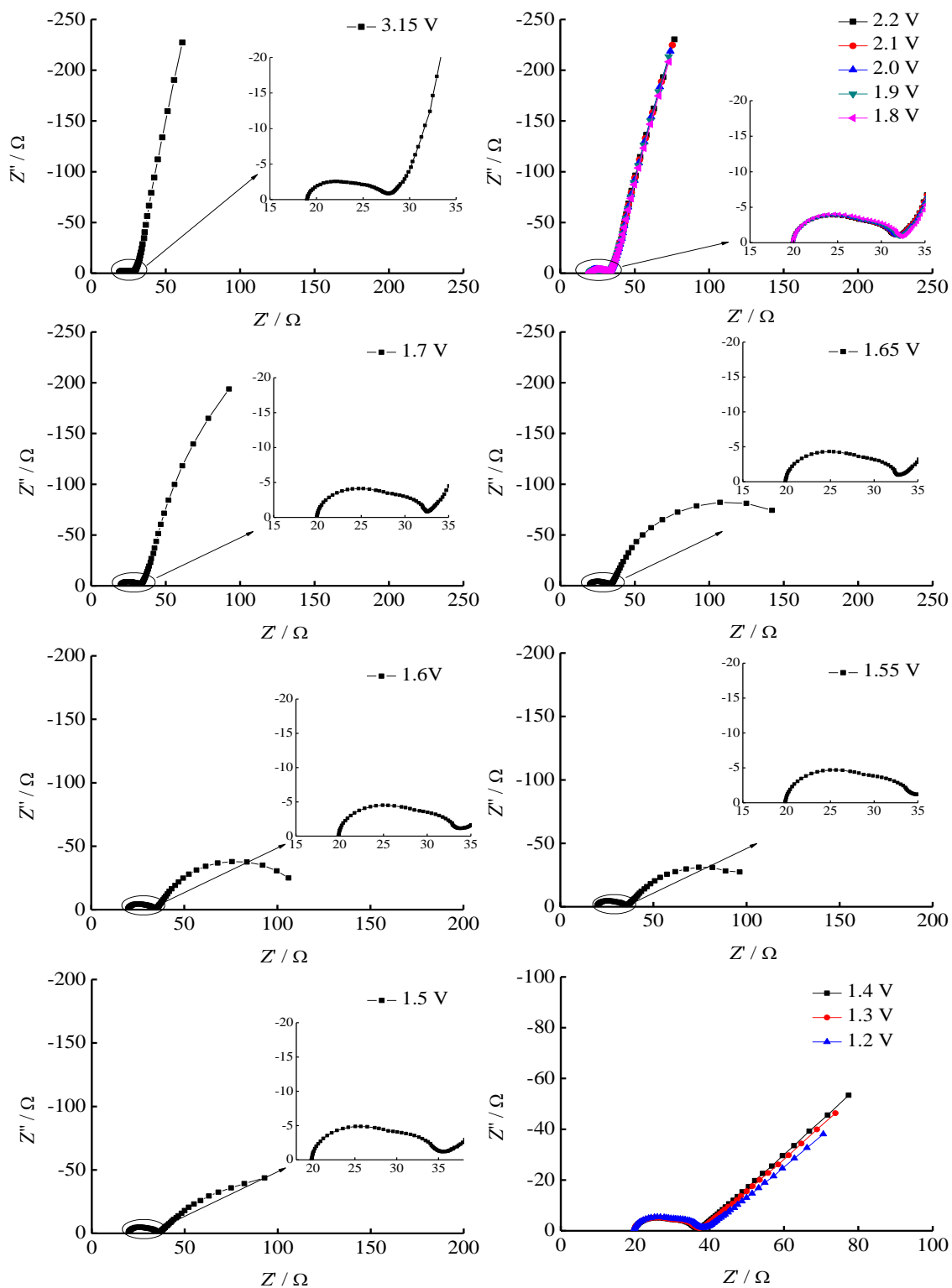
Figure 3. Nyquist plots of the NiF_2/C electrode at various potentials from 3.15 to 1.2 V during the first discharge.
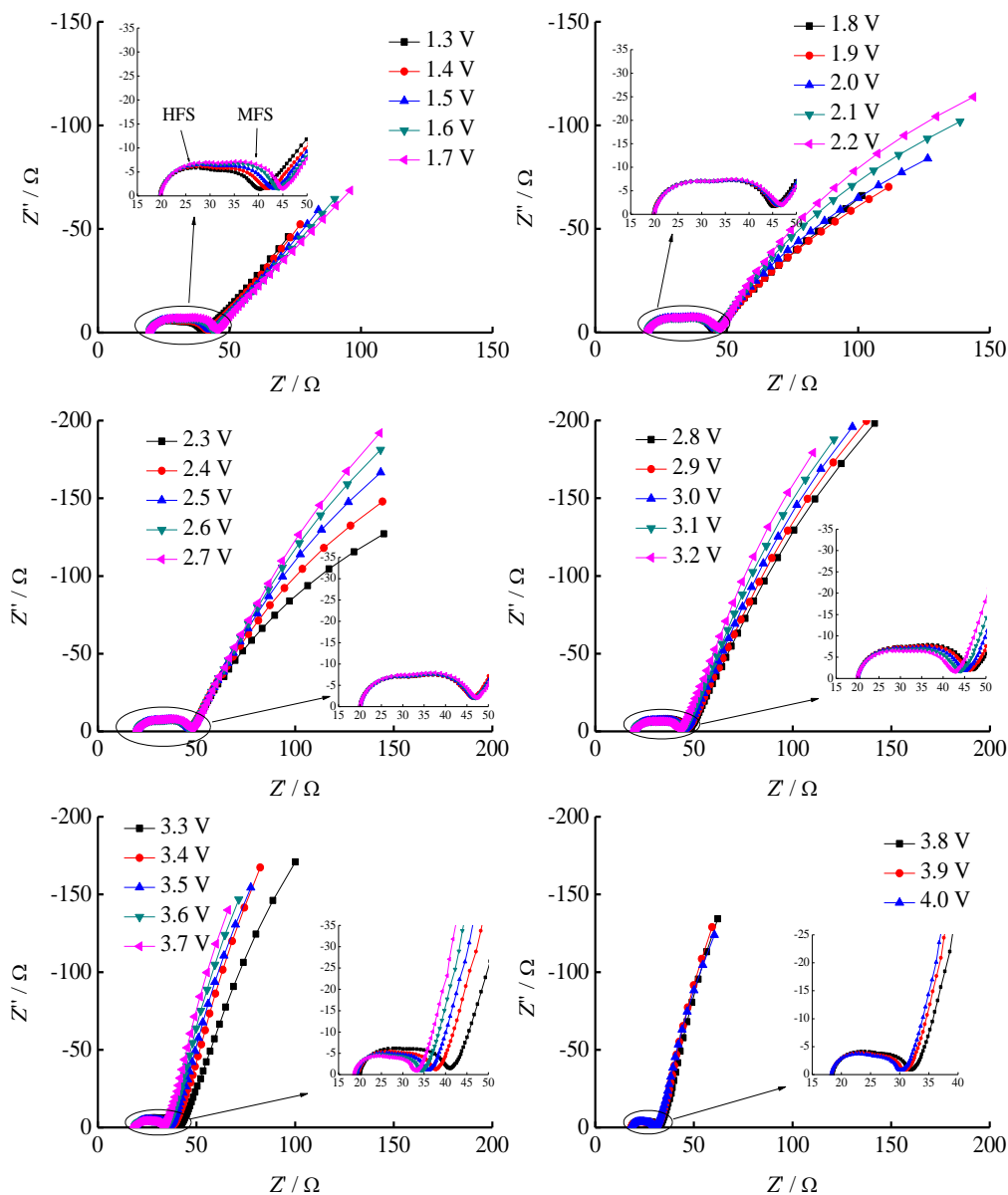
Figure 4. Nyquist plots of the NiF$_2$/C electrode at various potentials from 1.3 to 4.0 V during the first charge.

However, the peak potential of 2.0 V in the initial charge as well as the profile published before in literature [46], also below the theoretical lithiation voltage (2.96 V), indicates that the poor kinetic property of fluorides and the profile may cause the formation of NiO like composites to decrease the difficulties of converse reaction. As a result, the operating potentials would become lower in the subsequent cycles.

To investigate the the lithiation and delithiation conversion mechanisms of NiF$_2$/C composites at the electrode/electrolyte interface, EIS measurements were carried out for the NiF$_2$/C composites electrode during the first discharge-charge cycle. Figure 3 shows the Nyquist plots obtained from the NiF$_2$/C composites electrode in the potential region from 3.15 to 1.2 V during the first discharge

process, and the Nyquist plots of the first charge process in Figure 4 shows a converse course. The chosen potential region is based on the lithiation/delithiation conversion process, without concerning with the conditions at low potential (below 1 V). The Nyquist plot of NiF$_2$/C composites electrode at open circuit potential (3.15 V), gives a compressed and prolonged small semicircle which seems to be composed of two parts in the high-frequency (HF) to middle-frequency (MF) region, and a slightly inclined line in the low-frequency (LF) region. This phenomenon is similar to that of insertion materials, and the small semicircle in HF-MF region is related to SEI film (the resistance of SEI film coupled with SEI film capacitance), the slightly inclined line represents the blocking character of the nonlithiated electrode at equilibrium potential due to the large charge transfer resistance coupled with double capacitance. [23, 49-51].

Along with the decrease of the electrode polarization potential, the small semicircle in the HF-MF region appears to divide into two separated semicircles with the gradually growth of each part, while the inclined line in the LF region doesn't change significantly above 1.8V in the discharge process. With the potential changing from 1.8 to 1.5 V in the discharge process, the inclined line in the LF region, which is strongly potential dependent, shows an increasing tendency to move towards the real axis; and another semicircle is formed at 1.6 V, corresponding to the plateau in the voltage profile in the charge-discharge curves, further demonstrating that the inclined line or the semicircle in the LF region should be ascribed to the charge transfer step undoubtedly. On further discharge to 1.2 V, the semicircle in the LF region turns into an inclined line again below 1.4 V, indicating charge transfer proceeds hardly during those potentials.

An important feature of the impedance spectra is that the small semicircle in HF-MF region is evolved into two well separated semicircles in the charge process, displaying that the small semicircle in HF-MF region observed in the discharge process consists of two semicircles that overlapped each other due to that the differences in their time constants are too small.

Thus the spectra in the charge process can be distinguished in three sections, namely a semicircle in the HF region, a semicircle in the MF region and an inclined line or a semicircle in the LF region. As discussed above, the semicircle in the HF region and the inclined line or a semicircle in the LF region could be attributed to lithium ion migration through the SEI film covered on the active materials and charge transfer step, respectively. What could be the origin of the semicircle in the MF region? This will be discussed below in detail.

According to the experimental results obtained in this work, an equivalent circuit, as shown in Figure 5, is proposed to fit the impedance spectra of the NiF$_2$/C composites electrode in the first discharge-charge process. In this equivalent circuit, R_s represents the ohmic resistance of electrolyte; R_1, R_2, R_3 and constant phase elements (CPE) Q_1, Q_2, Q_3 represent the resistance and capacitance of the semicircle in the HF region, the semicircle in the MF region and the inclined line or semicircle in the LF region, respectively. The expression for the admittance response of the CPE (Q) is

$$Y = Y_0\omega^n \cos(\frac{n\pi}{2}) + jY_0\omega^n \sin(\frac{n\pi}{2}) \tag{3}$$

where ω is the angular frequency and j is the imaginary unit. A CPE represents a resistor when $n = 0$, a capacitor with capacitance of C when $n = 1$, an inductor when $n = -1$, and a Warburg resistance when $n = 0.5$.
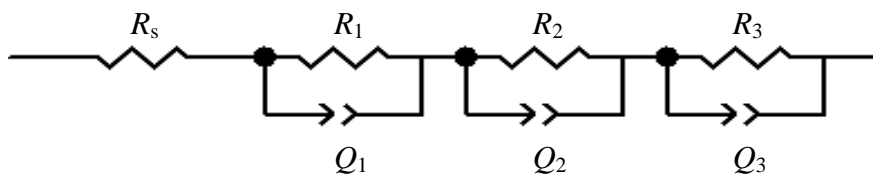
Figure 5. Equivalent circuit proposed for analysis of the NiF$_2$/C electrode in the first discharge-charge process.
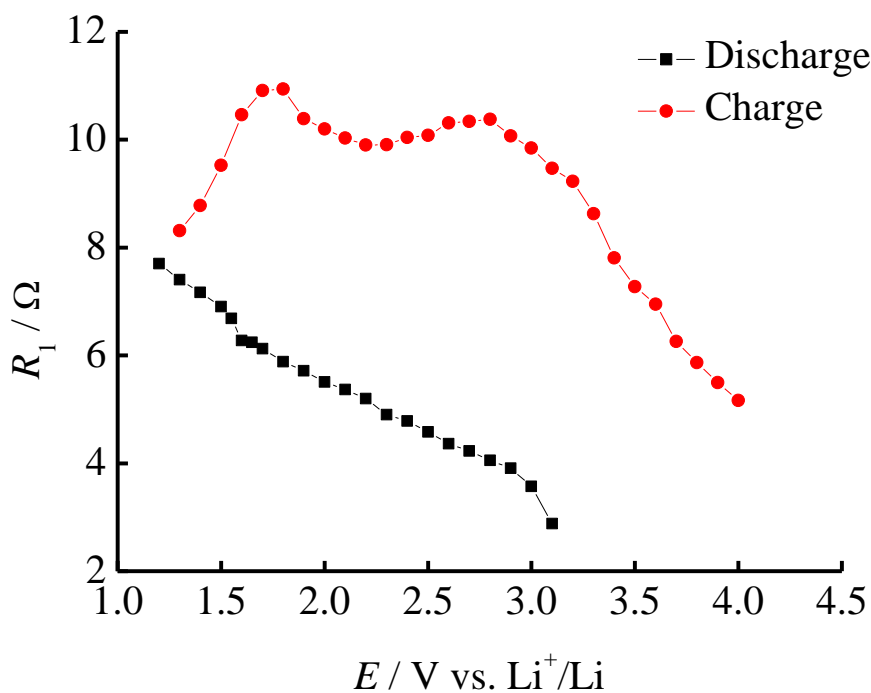
Figure 6. Variations of R_1 with electrode potential obtained from fitting the experimental impedance spectra of the NiF$_2$/C electrode during the first discharge-charge cycle.

Variations of R_1 corresponding to the semicircle in the HF region with the change of electrode polarization potential obtained from fitting the experimental impedance spectra of the NiF$_2$/C composites electrode in the first discharge-charge process are shown in Figure 6. As can be seen, R_1 increases continuously with the decrease of electrode polarization potential in the discharge process, signifying the increase of the thickness of SEI film. In the course of the subsequent charge, with the increase of electrode polarization potential, R_1 increases below 1.8 V. When the electrode polarization potential is changed from 1.8 to 2.8 V, R_1 decreases slowly; on further charging to 4.0 V, R_1 decreases rapidly, implying the decrease of the thickness of SEI film. The above phenomenon commonly attributes to the reversible formation/decomposition of SEI film covered on the transition metal

fluorides in the charge-discharge processes as suggested by Gmitter et al. [52], and similar phenomenon was also observed on Cr_2O_3 electrode by Li et al. [47, 48]. Since the thick SEI film covers all particles, it is believed that the reversible formation/decomposition of the SEI film is not favorable for achieving good cyclic performance. It may lead to the peeling off of active materials from the current collector [48].
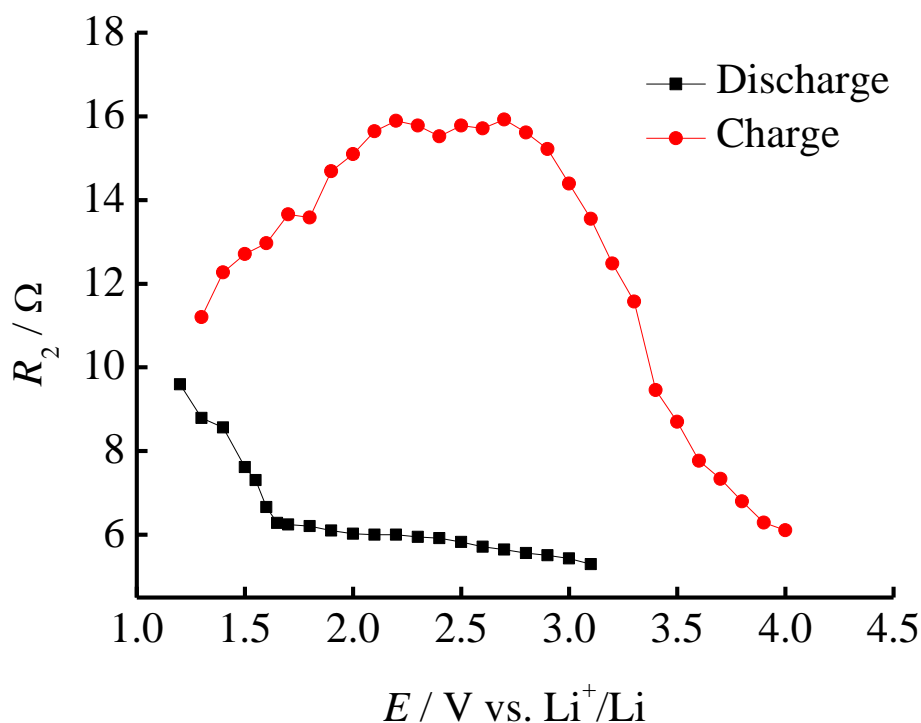
Figure 7. Variations of R_2 with electrode potential obtained from fitting the experimental impedance spectra of the NiF_2/C electrode during the first discharge-charge cycle.

Figure 7 illustrates variations of R_2 corresponding to semicircle in the MF region with the change of electrode polarization potential obtained from fitting the experimental impedance spectra of the NiF_2/C composites electrode in the first discharge-charge cycle. In our previous study [53], the processes of the first delithiation/lithiation of the spinel $LiMn_2O_4$ electrode were investigated by EIS. Three semicircles, which are similar to that of NiF_2/C composites obtained in this study, were also observed in the Nyquist diagram at intermediate degrees of intercalation, and the semicircle in the MF region is attributed to the electronic properties of the material, namely R_2 corresponds to the electronic resistance of the materials. However, most metal fluorides such as NiF_2 are insulators with large band gap, and the way of milling with conductive agent to form composites does not essentially improve the conductivity of materials themselves, therefore the transport of electrons in active materials is almost impossible. Moreover, R_2, the fitted values of MFS, with the value of only scores of ohms, could not be the reflection of the electronic resistance of NiF_2. Thus the semicircle in the MF region in Nyquist

plots obtained from the NiF_2/C composites could not be attributed to the electronic properties of the material as that obtained from the spinel $LiMn_2O_4$.

As introduced in experimental section, NiF_2/C composites electrode consists of NiF_2 and conductive materials such as carbon black and graphite. To physically hold the electrode together, a binder is also added. Since NiF_2 is insulator, the electron charge conduction through or out of the particles of NiF_2 must take place as follows: (a) the electrons are transported across the conductive material to the points where they meet the active material and the conductive material (b) then the electrons hop on the surface of the particles of NiF_2. It is well known that when a conductor is brought into contact with a semiconductor, a type of contact named Schottky contact will sometimes form to contribute resistance [54-56].

According to thermionic emission diffusion theory, a Schottky contact behaviour can be described by the equation which takes into account the defects of lattice, electric field, tunneling effects, the presence of an interfacial layer, and carrier recombination in the space charge region of the metal-semiconductor contact as given by [54-56]:

$$I = I_0 \exp(\frac{qE}{nkT})[1 - \exp(\frac{-qE}{kT})] \tag{4}$$

Where I_0 is the saturation current, q the electronic charge, k Boltzmann constant, T the absolute temperature, E the applied bias voltage, n is the ideal factor. The expression for the saturation current, I_0 is:

$$I_0 = AA^*T^2 \exp(-\frac{q\Phi_B}{kT}) \tag{5}$$

Where A is the Schottky contact area, A^* the effective Richardson constant, and $q\Phi_B$ is the Schottky barrier height. When $E > 3kT/q$, equation (4) can be simplified to:

$$I = I_0 \exp(\frac{qE}{nkT}) \tag{6}$$

According to the Ohm's Laws, the Schottky contact resistance R can be presented in the following form:

$$R = (\frac{dI}{dE})^{-1} \tag{7}$$

Substitute Equations (6) into Equation (7), R can be obtained in the following expression:

$$R = (I_0 \frac{q}{nkT})^{-1} \exp(-\frac{qE}{nkT}) \tag{8}$$

When the contact media do not change, A^* and Φ_B could be considered to be invariable, equation (8) could be written as:

$$R = C\exp(-\frac{qE}{nkT}) \tag{9}$$

Where C is constant. Therefore change equation (9) to linear equation by logarithm, we can obtain finally the following expression:

$$\ln R = \ln C - \frac{qE}{nkT} \tag{10}$$

The plot of $\ln R$ versus E should give a straight line with the slope $= -q/nkT$ and y-intercept at $\ln C$ on condition that no change occur with contact media.
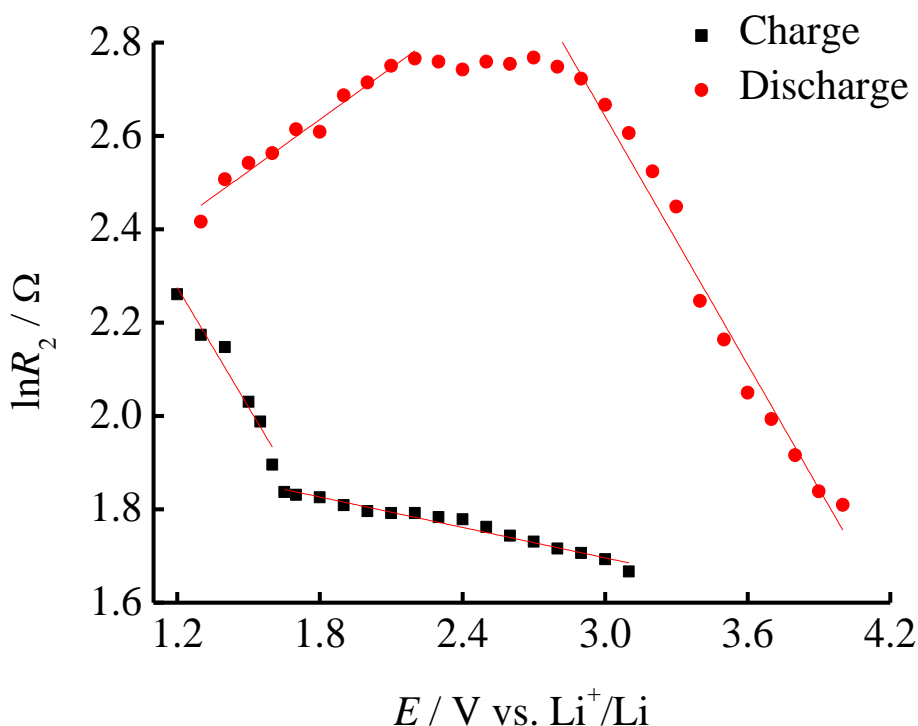
Figure 8. Comparison of $\ln R_2$-E with the linear fitting results

Figure 8 shows a comparison diagram of $\ln R_2$-E and the linear fitting results, which is well consistent with equation (10). There are two segments with different slopes and intercepts in the discharge and charge process respectively.

It can be clearly observed that the intersection potential of two segments in discharge process approaches to the potential of conversion reaction, indicating that the alternation of contact media after the reaction (2) ($2Li+NiF_2 \rightarrow Ni+2LiF$) result in the variation of Schottky barrier height (SBH) in I_0 and the ideal factor n. Similar phenomenon has been found in the charge process. However, some

points in Figure 8 between 2.3 to 2.8 V in the charge process appear to be nonlinear, which is probably caused by the proceeding of conversion reaction.

On the basis of the analysis above, it supports the assumption mentioned before, that the semicircle in the middle frequency region (MFS) should be related to the contact between conductive agents and active materials. In addition, different ideal factors *n* have been calculated with the value of 364.3, 46.2 in discharge process and -107.47, 44.6 in the charge process according to the slope value from fitting. The large deviation from ideal value of 1 signifies poor Schottky contact between NiF_2 and C, as well as the intermediate products after reaction including NiO and LiF in the composites electrode.
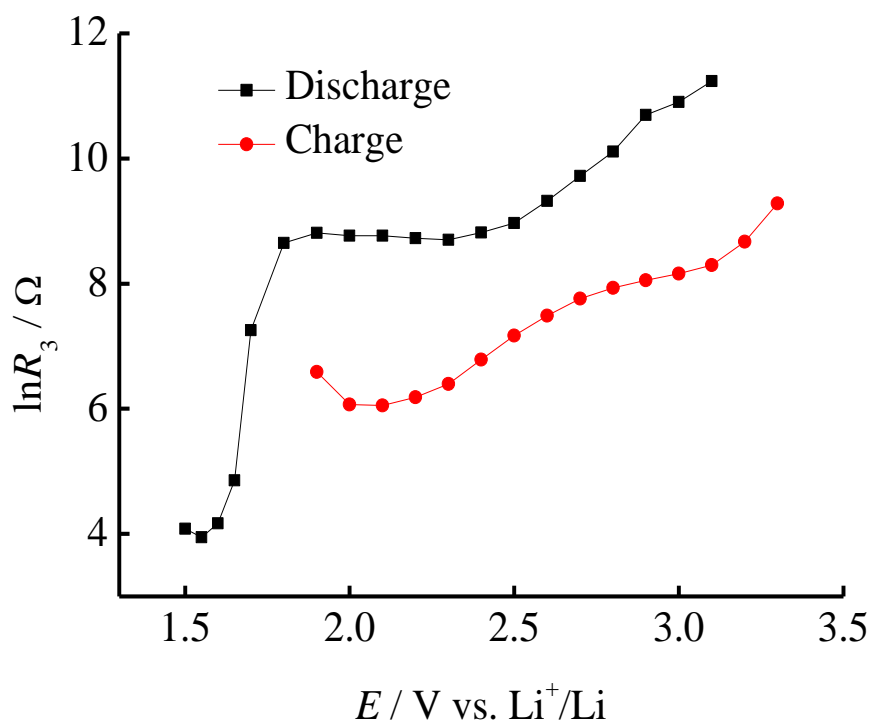
Figure 9. Variations of $\ln R_3$ with electrode potential obtained from fitting the experimental impedance spectra of the NiF_2/C electrode during the first discharge-charge cycle.

Variations of $\ln R_3$ with the change of electrode polarization potential are shown in Figure 9, which reflect the difficulty of electrochemical reaction. As the low-frequency arc turns into a sloping line in the 1.4 V - 1.2 V in discharge process and 1.3 V - 1.7 V in charge process, indicating the charge transfer process has already finished, the fitted values under these potentials are not given. It can be observed that R_3 reaches to the minimum at 1.6 V in discharge process and 2.0 V in charge process, respectively, in accordance with the result of charge-discharge test above. It is worth nothing that the minimum value of R_3 in charge process is much larger than that in discharge process, indicating that the subsequent charging process is more difficult. In addition, the Warburg impedance has not been detected in the low frequent region above 10^{-2} Hz under the reaction potential, which also differs from the typical characteristic of EIS of insertion/deinsertion compounds [23], probably due to the poor conductivity and kinetics of NiF_2.

4. PHYSICAL MECHANISMS OF LITHIATION AND DELITHIATION CONVERSION

During the past decades, some models have been proposed to explain the impedance response of the insertion materials for lithium ion batteries, including anode materials such as graphite and cathode materials such as $LiMn_2O_4$, $LiMnO_2$, $LiNiO_2$, and $LiCoO_2$. Among these models, the modified Voigt-FMG equivalent circuit, suggested by Aurbach et al., [40, 49, 57] is considered to provide the best account of the lithium ion insertion process in these materials. This model reflects the steps involved during lithium ion insertion: (*i*) lithium-ion transport in an electrolyte, (*ii*) lithium ion migration through the SEI film, (*iii*) charge-transfer through the electrode/electrolyte interface, (*iv*) lithium ion diffusion in an electrode, and (*v*) electron transport in an electrode and at an electrode/current collector interface. Among these steps of lithium ion insertion, the electron transport (*v*) and lithium-ion transport in the electrolyte solution (*i*) usually give no semicircle in the frequency range $10^5 \sim 10^{-2}$ Hz range due to their high characteristic frequencies, and these components of resistance appear as a Z' intercept in the Nyquist plot. The process (*iv*) gives the Warburg impedance, which was observed as a straight line with an angle of 45° from the Z' axis, and the other two processes (*ii*) and (*iii*) give their own semicircles at each characteristic frequency, respectively. Yet the above model is a simplification of real situation that the electrode is assumed to be built up of spherical particles of uniform size, and no change of the particle structure or new phase formation. Afterwards, Barsoukov et al. [23, 58] proposed a new model based on single particles for commercial electrode prepared by composites. They supposed that the electrochemical kinetics characteristic of battery materials is represented by several common steps: (*i*) ionic charge conduction through electrolyte in the pores of the active layer and electronic charge conduction through the conductive part of the active layer; (*ii*) Lithium ion diffusion through the surface insulating layer of the active material; (*iii*) electrochemical reaction on the interface of active material particles including electron transfer; (*iv*) lithium ion diffusion in the solid phase and (*v*) phase-transfer in cases where several phases are present and a capacitive behavior that is related to the occupation of lithium ions, which give a semicircle and straight line perpendicular to Z' axis in the Nyquist plot (commonly below 10^{-2} Hz), respectively. However, many electrochemically active materials are not good electronic conductors, and conductive agents should be essential, and the electron conduction in electrode materials is obviously underestimated by Barsoukov et al. In our previous work [53], a modified model is put forward based on the experimental results, and the EIS spectra in the frequency range $10^5 \sim 10^{-2}$ Hz are interpreted in terms of the following physical phenomena in an order of decreasing frequency: (*i*) a high frequency semicircle because of the presence of a surface layer, (*ii*) a middle to high frequency semicircle related to the electronic properties of the material, (*iii*) a middle frequency semicircle associated with charge transfer, and finally, (*iv*) the very low frequency incline line attributed to the solid state diffusion.

So far, the above models do provide the excellent interpretation of insertion/deinsertion reaction mechanism, however, the lithiation and delithiation conversion mechanism have been available rarely. According to the experimental results in this paper, three semicircles have been also observed in the EIS spectra which are similar to the results of insertion materials obtained in our previous study[53], including lithium ion diffusion through SEI film and charge transfer process, while electron transport in the electrode of NiF_2/C composites is utterly different. Since NiF_2 is totally

electronic insulator in room temperature, the electrochemical reaction can only occur at those points where they meet the conductive agents, so the electrical contact in the component materials is one of the most important issues in connection with the performance of batteries.
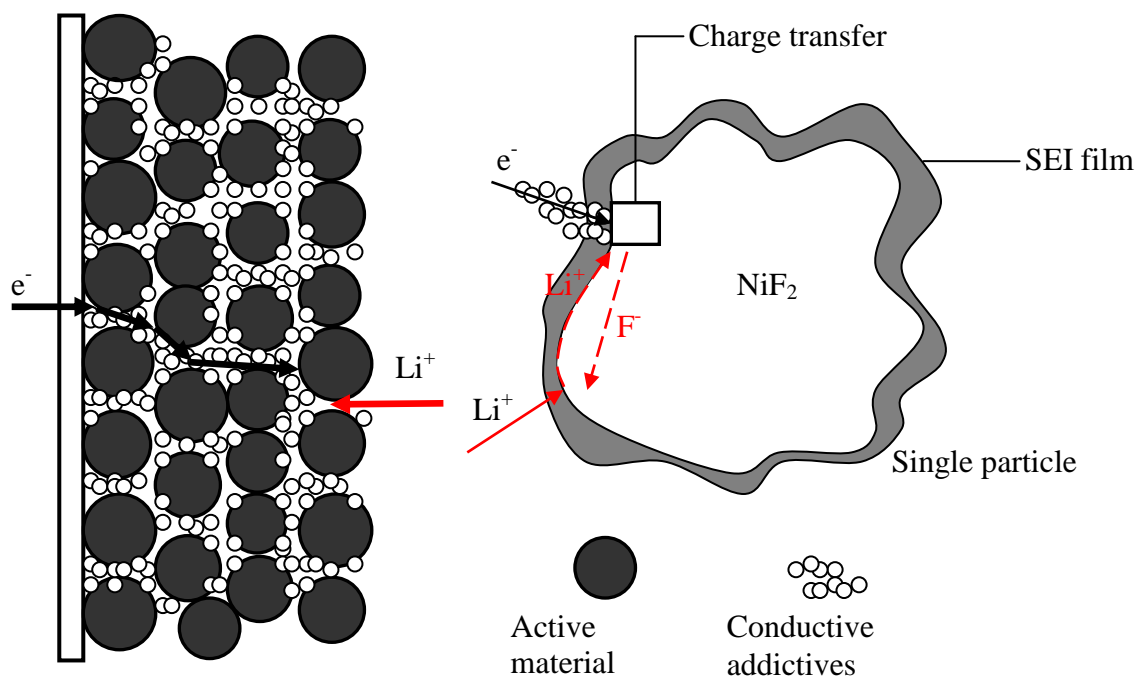
Figure 10. Pictorial representation model for NiF_2/C electrode based on conversion reaction

As analyzed above, a new model (Figure 10) is put forward, to explain the impedance response of the transition metal fluorides of lithium ion batteries, such as NiF_2. As can be seen from Figure 10, because the SEI film is ionically conducting but electronically insulating [33], it is possible that electron charge conduction out of the particles takes place as follows as mentioned above: (a) the electrons are transported across the conductive material to the points where they meet the active material and the conductive material (b) the electrons hop on the surface of the particles of NiF_2 through the Schottky contact. Consequently, it is reasonable that the EIS are interpreted in terms of the following physical phenomena in an order of decreasing frequency: firstly ionic charge conduct through electrolyte and lithium ions diffuse through the SEI film to the surface of the NiF_2; To maintain electrical neutrality of particles, electrons along the external circuit, conductive agents, and the contact points between NiF_2 and C, then hop on the surface of NiF_2. Later the charge transfer process takes place close to the carbon particles. But for the diffusion process, because F^- could migrate in the NiF_2 particles [59] and compete favorably with Li^+ [60], there may exist two ways: (i) Li^+ diffuses to contact points to form LiF along the particle surface; (ii) F^- migrates further from the carbon, through the NiF_2 phase, or along the newly formed Ni-NiF_2 interfaces, so as to the surface of NiF_2 and form LiF with Li^+.

5. CONCLUSIONS

The first discharge-charge process of NiF_2/C at different potentials has been investigated by electrochemical impedance spectroscopy. The results have revealed that the typical EIS characteristics appeared with three semicircles in the Nyquist diagram at 1.6V. It has been found that the three semicircles have been assigned to the migration of lithium ions through the SEI films, the transport of electrons in the contact points between NiF_2 and C, and the charge transfer step in an order of decreasing frequency, respectively. On the basis of the experimental results, a modified model has been put forward to explain the impedance response of NiF_2/C electrode for lithium ion batteries successfully.

References

1. J. M. Tarascon, M. Armand, *Nature*, 414 (2001) 359.
2. K. Mizushima, P. C. Jones, P. J. Wiseman, J. B. Goodenough, *Mater. Res. Bull.*, 15 (1980) 783.
3. M. M. Thackeray, W. I. F. David, P. G. Bruce, J. B. Goodenough, *Mater. Res. Bull.*, 18 (1983) 461.
4. J. M. Tarascon, E. Wang, F. K. Shokoohi, W. R. McKinnon, S. Colson, *J. Electrochem. Soc.*, 138 (1991) 2859.
5. A.K. Padhi, K. S. Nanujundaswamy, J. B. Goodenough, *J. Electrochem. Soc.*, 144 (1997) 1188.
6. I.Plitz, F. Badway, J. Al-Sharab, A. DuPasquier, F. Cosandey, G. G. Amatucci, *J. Electrochem. Soc.*, 152 (2005) A307.
7. P. Poizot, S. Laruelle, S. Grugeon, L. Dupont, J. M. Tarascon, *Nature*, 407 (2000) 496.
8. N. Pereira, L. Dupont, J. M. Tarascon, L. C. Klein, G. G. Amatucci, *J. Electrochem. Soc.*, 150 (2003) A1273.
9. N. Pereira, L. C. Klein, G. G. Amatucci, *J. Electrochem. Soc.*, 149 (2002) A262.
10. A.Débart, L. Dupont, R. Patrice, J. M. Tarascon, *Solid State Sci.*, 8 (2006) 640.
11. D. C. S. Souza, V. Pralong, A. J. Jacobson, L. F. Nazar, *Science*, 296 (2002) 2012.
12. B. Mauvernay, M. L. Doublet, L. Monconduit, *J. Phys. Chem. Solids*, 67 (2006) 1252.
13. D. C. C. Silva, O. Crosnier, G. Ouvrard, J. Greedan, A. Safa-Sefat, L. F. Nazar, *Electrochem. Solid-State Lett.*, 6 (2003) A162.
14. M. Z. Xue, Z. W. Fu, *Electrochem. Commun.*, 8 (2006) 1855.
15. F. Badway, N. Pereira, F. Cosandey, G. G. Amatucci, *J. Electrochem. Soc.*, 150 (2003) A1209.
16. F. Badway, F. Cosandey, N. Pereira, G. G. Amatucci, *J. Electrochem. Soc.*, 150 (2003) A1318.
17. P. Liao, B. L. MacDonald, R. A. Dunlap, J. R. Dahn, *Chem. Mater.*, 20 (2008) 454.
18. R. E. Doe, K. A. Persson, Y. S. Meng, G. Ceder, *Chem. Mater.*, 20 (2008) 5274.
19. S. Mitra, P. Poizot, A. Finke, J. M. Tarascon, *Adv. Funct. Mater.*, 16 (2006) 2281.
20. H. Li, Z. X. Wang, L. Q. Chen, X. J. Huang, *Adv. Mater.*, 21 (2009) 4593.
21. N. Yamakawa, M. Jiang, B. Key, C. P. Grey, *J. Am. Chem. Soc.*, 131 (2009) 10525.
22. R. F. Li, S. Q. Wu, Y. Yang, Z. Z. Zhu, *J. Phys. Chem. C*, 114 (2010) 16813.

23. E. Barsoukov, D. H. Kim, H.-S. Lee, H. Lee, M. Yakovleva, Y. Gao, J. F. Engel, *Solid State Ionics*, 161 (2003) 19.
24. A.Kazakopoulos, C. Sarafidis, K. Chrissafis, O. Kalogirou, *Solid State Ionics*, 179 (2008) 1980.
25. M. D. Levi, D. Aurbach, *J. Phys. Chem. B*, 109 (2005) 2763.
26. T. Doi, T. Yahiro, S. Okada, J. -i. Yamaki, *Electrochim. Acta*, 53 (2008) 8064.
27. D. Aurbach, M. D. Levi, E. Levi, *Solid State Ionics*, 179 (2008) 742.
28. M. Itagaki, N. Kobari, S. Yotsuda, K. Watanabe, S. Kinoshita, M. Ue, *J. Power Sources*, 148 (2005) 78.
29. K. Dokko, M. Mohamedi, M. Umeda, I. Uchida, *J. Electrochem. Soc.*, 150 (2003) A425.
30. S. Kobayashi, Y. Uchimoto, *J. Phys. Chem. B*, 109 (2005) 13322.
31. F. Croce, F. Nobili, A. Deptula, W. Lada, R. Tossici, A. D'Epifanio, B. Scrosati, R. Marassi, *Electrochem. Commun.*, 1 (1999) 605.
32. M. Morita, O. Yamada, M. Ishikawa, *J. Power Sources*, 81-82 (1999) 425.
33. A.-K. Hjelm, G. Lindbergh, *Electrochim. Acta*, 47 (2002) 1747.
34. M. Mohamedi, D. Takahashi, T. Itoh, M. Umeda, I. Uchida, *J. Electrochem. Soc.*, 149 (2002) A19.
35. K. A. Striebel, E. Sakai, E. J. Cairns, *J. Electrochem. Soc.*, 149 (2002) A61.
36. K. Dokko, M. Mohamedi, M. Umeda, I. Uchida, *J. Electrochem. Soc.*, 150 (2003) A425.
37. F. Nobili, R. Tossici, R. Marassi, F. Croce, B. Scrosati, *J. Phys. Chem. B*, 106 (2002) 3909.
38. M. Nakayama, H. Ikuta, Y. Uchimoto, M. Wakihara, *J. Phys. Chem. B*, 107 (2003) 10603.
39. D. Aurbach, M. D. Levi, E. Levi, H. Telier, B. Markovsky, G. Salitra, U. Heider, L. Hekier, *J. Electrochem. Soc.*, 145 (1998) 3024.
40. D. Aurbach, K. Gamolsky, B. Markovsky, G. Salitra, Y. Gofer, U. Heider, R. Oesten, M. Schmidt, *J. Electrochem. Soc.*, 147 (2000) 1322.
41. B. J. Johnson, D. H. Doughty, J. A. Voigt, T. J. Boyle, *J. Power Sources*, 68 (1997) 634.
42. S. Denis, E. Baudrin, F. Orsini, G. Ouvrard, M. Touboul, J. M. Tarascon, *J. Power Sources*, 81 (1999) 79.
43. H. Li, P. Balaya, J. Maier, *J. Electrochem. Soc.*, 151 (2004) A1878.
44. H. Li, G. Richter, J. Maier, *Adv. Mater.*, 15 (2003) 736.
45. S. Laruelle, S. Grugeon, P. Poizot, M. Dolle, L. Dupont, J. M. Tarascon, *J. Electrochem. Soc.*, 149 (2002) A627.
46. H. Zhang, Y. N. Zhou, Q. Sun, Z. W. Fu, *Solid State Sciences*, 10 (2008) 1166.
47. J. Hu, H. Li, X. J. Huang, L. Q. Chen, *Solid State Ionics*, 177 (2006) 2791.
48. J. Hu, H. Li, X. J. Huang, Electrochem. *Solid-State Lett.*, 8 (2005) A66.
49. M. D. Levi, D. Aurbach, *J. Phys. Chem. B*, 101 (1997) 4630.
50. M. Holzapfel, A. Martinent, F. Alloin, B. Le Gorrec, R. Yazami, C. Montella, *J. Electroanal. Chem.*, 546 (2003) 41.
51. J. S. Gnanaraj, R. W. Thompson, S. N. Iaconatti, J. F. DiCarlo, K. M. Abrahamb, *Electrochem. Solid-State Lett.*, 8 (2005) A128.
52. A.J. Gmitter, F. Badway, S. Rangan, R. A. Bartynski, A. Halajko, N. Pereira, G. G. Amatucci, *J. Mater. Chem.*, 20 (2010) 4149.
53. Q. C. Zhuang, T. Wei, L. L. Du, Y. L. Cui, L. Fang, S. G. Sun, *J. Phys. Chem. C*, 114 (2010) 8614.
54. S. M. Sze, *Physics of Semiconductor Devices, second ed,* Wiley, New Jersey (1981).
55. E. H. Rhoderick, R. H. Williams, *Metal-Semiconductor Contacts*, Clarendon, Oxford (1988).
56. H. C. Card, E. H. Rhoderick, *J. Phys. D*, 4 (1971) 1589.
57. B. Markovsky, M. D. Levi, D. Aurbach, *Electrochim. Acta*, 43 (1998) 2287.
58. E. Barsoukov, J. H. Kim, J. H. Kim, C. O. Yoon, H. Lee, *Solid State Ionics*, 116 (1999) 249.
59. K. J. W. Atkinson, R. W. Grimes, S. L. Owens, *Solid State Ionics*, 150 (2002) 443.
60. N. Yamakawa, M. Jiang, C. P. Grey, *Chem. Mater.*, 21 (2009) 3162.